minerals

MDPI

Communication

Gypsum Amendment Induced Rapid Pyritization in Fe-Rich Mine Tailings from Doce River Estuary after the Fundão Dam Collapse

Amanda D. Ferreira [1], Hermano M. Queiroz [1], Maira P. Kaneagae [1], Gabriel N. Nóbrega [2], Xosé L. Otero [3], Ângelo F. Bernardino [4] and Tiago O. Ferreira [1,*]

1 Department of Soil Science, College of Agriculture Luiz de Queiroz, University of São Paulo, ESALQ/USP, Av. Pádua Dias 11, Piracicaba SP 13418, Brazil; amandaduim@usp.br (A.D.F.); hermanomelo@usp.br (H.M.Q.); maira.kanegae@usp.br (M.P.K.)
2 Graduate Program in Geoscience (Geochemistry), Department of Geochemistry, Federal Fluminense University, Outeiro de São João Batista s/n, Campus do Valonguinho, Centro, Niterói RJ 24020, Brazil; gabrielnn@id.uff.br
3 Department of Edaphology and Agricultural Chemistry—CRETUS, Faculty of Biology, Universidad de Santiago de Compostela, Campus Sur, 15782 Santiago de Compostela, Spain; xl.otero@usc.es
4 Grupo de Ecologia Bentônica, Departamento de Oceanografia, Universidade Federal do Espírito Santo, Vitória, Espírito Santo 29075-910, Brazil; bernardino.ufes@gmail.com
* Correspondence: toferreira@usp.br

Abstract: Mine tailings containing trace metals arrived at the Doce River estuary, after the world's largest mine tailings disaster (the Mariana disaster) dumped approximately 50 million m^3 of Fe-rich tailings into the Doce River Basin. The metals in the tailings are of concern because they present a bioavailability risk in the estuary as well as chronic exposure hazards. Trace metal immobilization into sulfidic minerals, such as, pyrite, plays a key role in estuarine soils; however, this process is limited in the Doce River estuarine soil due to low sulfate inputs. Thus, to assess the use of gypsum amendment to induce pyritization in deposited tailings, a mesocosm experiment was performed for 35 days, with vinasse added as carbon source and doses of gypsum (as a sulfate source). Chemical and morphological evidence of Fe sulfide mineral precipitation was observed. For instance, the addition of 439 mg of S led to the formation of gray and black spots, an Fe^{2+} increase and decrease in sulfides in the solution, an increase in pyritic Fe, and a greater Pb immobilization by pyrite at the end of the experiment. The results show that induced pyritization may be a strategy for remediating metal contamination at the Doce River estuary.

Keywords: sulfidation; pyrite; lead sulfide; soil remediation; chemical immobilization

check for updates

Citation: Ferreira, A.D.; Queiroz, H.M.; Kaneagae, M.P.; Nóbrega, G.N.; Otero, X.L.; Bernardino, Â.F.; Ferreira, T.O. Gypsum Amendment Induced Rapid Pyritization in Fe-Rich Mine Tailings from Doce River Estuary after the Fundão Dam Collapse. *Minerals* **2021**, *11*, 201. https://doi.org/10.3390/min11020201

Received: 31 December 2020
Accepted: 10 February 2021
Published: 14 February 2021

Publisher's Note: MDPI stays neutral with regard to jurisdictional claims in published maps and institutional affiliations.

Copyright: © 2021 by the authors. Licensee MDPI, Basel, Switzerland. This article is an open access article distributed under the terms and conditions of the Creative Commons Attribution (CC BY) license (https://creativecommons.org/licenses/by/4.0/).

1. Introduction

The mineral pyrite (FeS_2) is widely known for its potential for metal immobilization in coastal wetland soils [1–4]. The formation of pyrite in soils is controlled by edaphic factors such as iron (Fe) and sulfide concentration in soil solutions, soil organic matter, microbial activity, redox potential (Eh), pH, soil moisture [5–8]. The formation of pyrite in coastal wetland soils results from anaerobic metabolic pathways for the degradation of organic matter using electron acceptors other than O_2 under reducing conditions (e.g., Eh < 100 mV) [5]. Accordingly, due to the high abundance of Fe and sulfate (SO_4^{2-}) from the ocean, the microbial reduction of Fe^{3+} and SO_4^{2-} is the most important anaerobic process for organic matter degradation in coastal wetlands soils [9,10]. In this sense, inducing the pyritization in soil has been identified as a strategy for increasing metal immobilization [11,12].

Since 2015, when the Fundão tailings dam in Brazil collapsed (the largest dam failure of the world, known as "Mariana disaster"), metal contamination has been identified as one

of the most concerning phenomena along the Brazilian Coast [13–17]. After the Mariana disaster, a huge amount of Fe-rich mining tailings entered the Doce River estuary increasing the trace metal content in the soil [14]. Furthermore, the biogeochemical conditions of the estuarine soils have since shown an increase in trace metal bioavailability due to the dissimilatory Fe reduction process [14,16,18]. Additionally, due to geomorphological conditions, the Doce River estuary presents some unique characteristics such as low levels of seawater intrusion and salinity, which reduce the occurrence of sulfate reduction and increase the contamination risks [14,16].

According to the US Environmental Protection Agency (EPA) toxicity classifications, soils at River Doce estuary can be classified as highly polluted with Pb (Table 1) since the concentration of this toxic element in the estuarine mine tailing deposits is 48.8% higher than the threshold effect level (TEL) (35 mg kg^{-1}) [19]. Lead (Pb) poisoning is a global concern and sulfidation of Pb is a relevant sink [4] because Pb is a metallic ion from "class B" or "soft sphere" and has a high affinity for forming strong soluble complexes with bisulfides and polysulfides [4].

Table 1. Chemical characterization of mine tailings.

pH	Eh *	TOC	TN	Sand	Silt	Clay	Fe	Al
	mV				%			
6.0	360	0.37	0.03	16.2	42.8	41.0	8.02	0.31
Mn	**Ba**	**Cd**	**Cr**	**Co**	**Cu**	**Ni**	**Pb**	**Zn**
				$mg \cdot kg^{-1}$				
854.92	95.44	6.03	20.79	20.08	24.75	7.88	68.41	86.27

* Eh: redox potential; TOC: total organic carbon; TN: total nitrogen.

Thus, improving pyritization through sulfur amendment is a useful strategy for inducing pedogenetic processes (i.e., sulfidation), and forming a Technosol, which can provide valuable ecosystem services, such as metal contamination remediation. In this sense, this study aimed to evaluate the use of different amendments to promote pyritization and reduce trace metal bioavailability from the Mariana disaster, supporting future estuarine reclamation.

Chemical immobilization is one of the most efficient in situ remediation techniques, especially when it uses cost-effective soil amendments [20,21]. We used gypsum ($CaSO_4$), a waste product of the phosphorus fertilizer industry, as a source of sulfate and vinasse, a waste from the sugarcane industry, as a source of carbon. These two waste materials were chosen because of their abundance and chemical characteristics, but also because of their low cost reduces the cost of remediation efforts [22,23]. For instance, gypsum is easily solubilized, which facilitates its action as a sulfate source in the field [24], whereas vinasse is rich in low molecular weight organic compounds (e.g., glycerol, lactic acid, ethanol, acetic acid, fructose, glucose, and sucrose) that are easily decomposed [25].

Therefore, we hypothesized that gypsum can be used as a source of sulfate for pyritization in Fe-rich mine tailings deposited in the Doce River estuary and that there is an optimum dose of gypsum for increasing pyritization. To test these hypotheses, we carried out mesocosm experiments for 35 days using mine tailings, with additions of vinasse and varying gypsum doses.

2. Materials and Methods

2.1. Site Characterization

Mine tailings were collected in August 2019 in the Doce River estuary in Regência, Espirito Santo state, Brazil (Figure 1A). Since 2015, the Doce River estuary has been affected by mine tailings from the "Fundão" dam collapse. A thin layer of tailings (almost 5 cm) within the estuary was recognized 15 days after the tailings' arrival in Regência [14].

In August 2019, mine tailings deposited on islands in the estuary reached over 30 cm (Figure 1B). In 2015 pseudo-total Fe, previously reported by [14], was 8.8 times higher than the pseudo-total Fe in the tailings collected in 2019. The water of the Doce River estuary has low salinity and a low sulfate content [17], which increases the risks of metal pollution through the microbial reduction of Fe and a lack of sulfate reduction to precipitate pyrite. This corroborates the low degree of pyritization in the estuary (<1%) reported by [14]. To evaluate the use of gypsum and vinasse as soil amendments we conducted a mesocosm experiment whereby different doses of gypsum and vinasse were added to mine tailings.

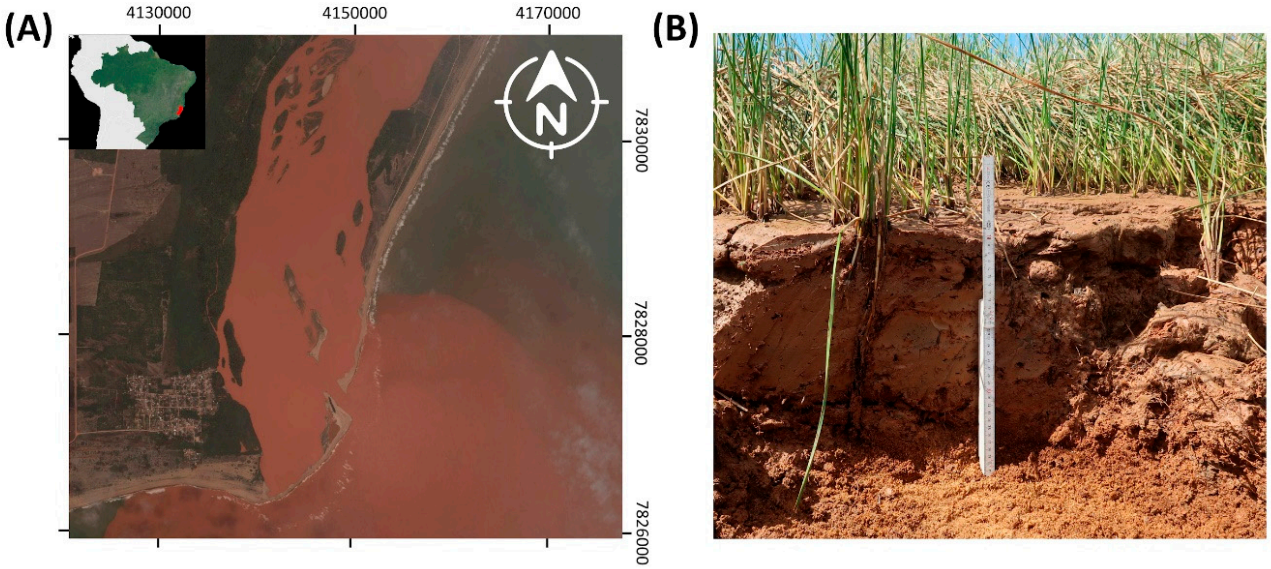

Figure 1. Location of the Doce River estuary, Espirito Santo state, affected by mine tailings (**A**) and a close-up of the mine tailings deposited on the estuarine soil in 2019 (**B**). In the image on the left (**A**), the XY axes represent UTM coordinates.

2.2. Characterization of Mine Tailings and Amendments

Samples of mine tailings deposited at the Doce River estuary were stored at approximately 4 °C in a laboratory to prevent chemical and biological alterations [18]. During the sampling procedure, redox potential (Eh) and pH values were determined using a platinum electrode and a previously calibrated glass electrode, respectively. The collected mine tailings were characterized according to their particle size distribution, mineralogical composition, organic carbon content, nitrogen content, and total metal content (Table 1).

The particle size distribution of mine tailings was determined using the pipette method [26]. The mine tailing mineralogical assemblage was determined using X-ray diffraction (XRD) with Cu-Kα radiation, at 0.02° 2θ s^{-1} in the range of 3–60° 2θ. The XRD analysis was performed using non-oriented powder mine tailings (Supplementary Figure S1). The total organic carbon (TOC) and nitrogen (TN) contents were obtained using an elementary analyzer (LECO 144 SE-DR, TrusPec®, Saint Joseph, MI, USA) [27]. The total metal contents were obtained after tri-acid digestion in a microwave using the Environmental Protection Agency (EPA) method 3052 [28] and determined by Inductively coupled plasma optical emission spectrometry (ICP-OES) (Thermo Fisher Scientific, Waltham, MA, USA), according to the 6010C protocol [29]. Prior to the mesocosm experiment, the gypsum and vinasse were chemically characterized [30], in terms of pH and TOC, as well as TN, P, K, Mg, Ca, and S content (Table 2).

Table 2. Chemical characterization of gypsum and vinasse.

	pH	C	N	P	K	Mg	Ca	S (SO^{2-}_4)
					g·kg^{-1}			
Gypsum				-			223.2	174.6
Vinasse	4.10	8.34	0.66	0.18	1.90	0.16	0.48	0.38

2.3. Experimental Design

A mesocosm experiment composed of six treatments was analyzed weekly for 35 days to evaluate pyrite formation after the addition of gypsum and vinasse. he mine tailings (25 g) were incubated in 50 mL Falcon® tubes, in triplicate, forming a factorial scheme, composed of 6 treatments and 5 evaluation times (destructive samples obtained weekly), totaling 90 experimental units (Figure 2). The treatments were set up as follows:

- Control: only deionized water (0 mg of S);
- Vinasse: only 6.2 mL of vinasse addition (as a carbon source: 51.7 mg of C, but with 2.4 mg of S);
- Vin + G1: 6.2 mL of vinasse + 0.5 g of gypsum (89.7 mg of S);
- Vin + G2: 6.2 mL of vinasse + 2.5 g of gypsum (439 mg of S);
- Vin + G3: 6.2 mL of vinasse + 5 g of gypsum (875 mg of S);
- Vin + G4: 6.2 mL of vinasse + 10 g of gypsum (1748 mg of S).

The treatments were randomized. The experimental units were maintained at a controlled temperature (25 ± 2 °C) and covered with aluminum foil to block any light. The aluminum foil cover was removed, and the tubes opened only during the evaluations.

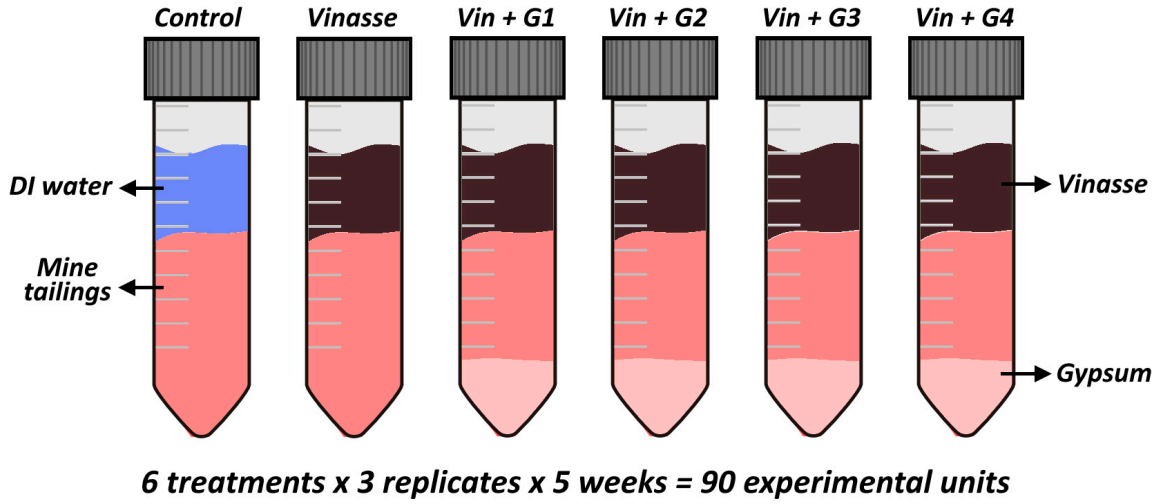

Figure 2. Design of mesocosms experiment and treatments. Control: only deionized water (0 mg of S); Vinasse: only vinasse addition (as a carbon source, but with 2.4 mg of S); Vin + G1: vinasse + 0.5 g of gypsum (89.7 mg of S); Vin + G2: vinasse + 2.5 g of gypsum (439 mg of S); Vin + G3: vinasse + 5 g of gypsum (875 mg of S); Vin + G4: vinasse + 10 g of gypsum (1748 mg of S).

2.4. Aqueous and Solid-Phase Analysis

Solution aliquots were collected weekly from mesocosm experiments to determine the concentration of dissolved Fe^{2+} [31], sulfides (HS^- and H_2S) [32] and Pb [29].

Destructive samples were collected weekly for Fe and Pb solid-phase fractionation analysis. Geochemical fractionation was carried out using a combination of methods proposed by [33–35], which enable the extraction of six operationally distinct fractions:

Exchangeable and soluble metals (EX) were extracted after 30 min (min) of agitation in 30 mL of 1 mol·L^{-1} $MgCl_2$ solution (pH 7.0).

Metals associated with carbonates (CA) were extracted after 5 h of agitation in 30 mL of 1 mol·L^{-1} NaOAc solution (pH 5.0).

Fe and other metals associated with ferrihydrite (FR) were extracted after 6 h at 30 °C of agitation in 30 mL of hydroxylamine solution 0.04 mol·L^{-1} + 25% acetic acid (vol/vol) solution.

Fe and other metals associated with lepidocrocite (LP) were extracted after 6 h at 96 °C of agitation in 30 mL of hydroxylamine solution 0.04 mol·L^{-1} + 25% acetic acid (vol/vol) solution.

Fe and other metals associated with goethite/hematite (OX) were extracted after 30 min at 75 °C of agitation in 20 mL of 0.25 mol·L^{-1} sodium citrate + 0.11 mol·L^{-1} sodium bicarbonate with 3 g of sodium dithionite.

Fe and other metals associated with pyrite (PY) were extracted after eliminating the Fe and metals associated with silicates (using 10 mol·L^{-1} HF) and the organic material (using concentrated H_2SO_4), the pyritic phase was extracted by shaking the residue for 2 h at room temperature with 10 mL of concentrated HNO_3. A more detailed description of the combined method is presented in [3,36]. Using this method, it is possible to calculate the degree of pyritization (DOP, %) and degree of trace metals pyritization (DTMP, %), which represent the proportion of pseudo-total contents incorporated into pyrite, as follows:

$$\mathrm{DOP}\ (\%) = \frac{\mathrm{Fe} - \mathrm{PY}}{\Sigma\,\mathrm{Fe} - \mathrm{EX} \rightarrow \mathrm{Fe} - \mathrm{PY}} \times 100 \quad (1)$$

$$\mathrm{DTMP}\ (\%) = \frac{\mathrm{ME} - \mathrm{PY}}{\Sigma\,\mathrm{ME} - \mathrm{EX} \rightarrow \mathrm{ME} - \mathrm{PY}} \times 100 \quad (2)$$

where $\mathrm{Fe} - \mathrm{PY}$ and $\mathrm{ME} - \mathrm{PY}$ is the concentration of Fe and other metals associated with the pyritic fraction (PY, in mg kg^{-1}), $\Sigma \mathrm{Fe} - \mathrm{EX} \rightarrow \mathrm{Fe} - \mathrm{PY}$ is the sum of all Fe fractions and $\Sigma\,\mathrm{ME} - \mathrm{EX} \rightarrow \mathrm{ME} - \mathrm{PY}$ is the sum all respective metal fractions.

2.5. Statistical Analysis

Variables were subjected to the non-parametric Kruskal–Wallis test to assess differences between treatments with the level of significance set to $p < 0.05$ (XLSTAT version 2014.5.03) [37]. Spearman correlation analysis was performed, and a model for trace metal pyritization was obtained using mixed-effect linear models through stepwise backward elimination. These analyses were performed in R [38].

3. Results and Discussion

3.1. Effects of Time and Amendment Dose

Pb in the aqueous phase was lower than the detection limit (0.01 mg·L^{-1}) in all treatments. Significant differences in the behavior of oxygen-sensitive chemical species (reduced iron, Fe^{2+}, and sulfide species, HS^- and H_2S) were observed in treatments over time (Table S1). The Fe^{2+} concentrations increased from the third week, especially in treatments including gypsum (Figure 3), followed by a decrease in the Fe^{2+} concentration from the fourth week. H_2S and HS^- concentrations exhibited similar behavior to Fe^{2+} with a significant increase from the second week and followed by a decrease (Figure 3). The addition of more gypsum resulted in more Fe^{2+} in the liquid phase, but the sulfide maximum concentration was observed with the Vin + G2 treatment (439 mg of S).

The increase in Fe^{2+} and sulfide concentration indicates the Fe^{3+} and SO_4^{2-} reduction processes, whereas the subsequent decrease in their concentration indicates precipitation [7]. Previous studies have reported models of pyritization [7,39] showing that dissolved Fe^{2+} reacts with HS^- and precipitates as FeSx species, such as mackinawite, greigite or other acid volatile sulfides (AVS), and pyrite [40,41]. The pathway of pyrite formation is very dependent on the Fe/S molar ratio and an excess of Fe^{2+} is required to precipitate FeS_2 [7,38]. In our experiment, the sulfide concentration in the solution was in the range of 29–600 µM, representing common sulfide concentration in coastal wetland soils and sediments [36,42–44], and allowing pyritization.

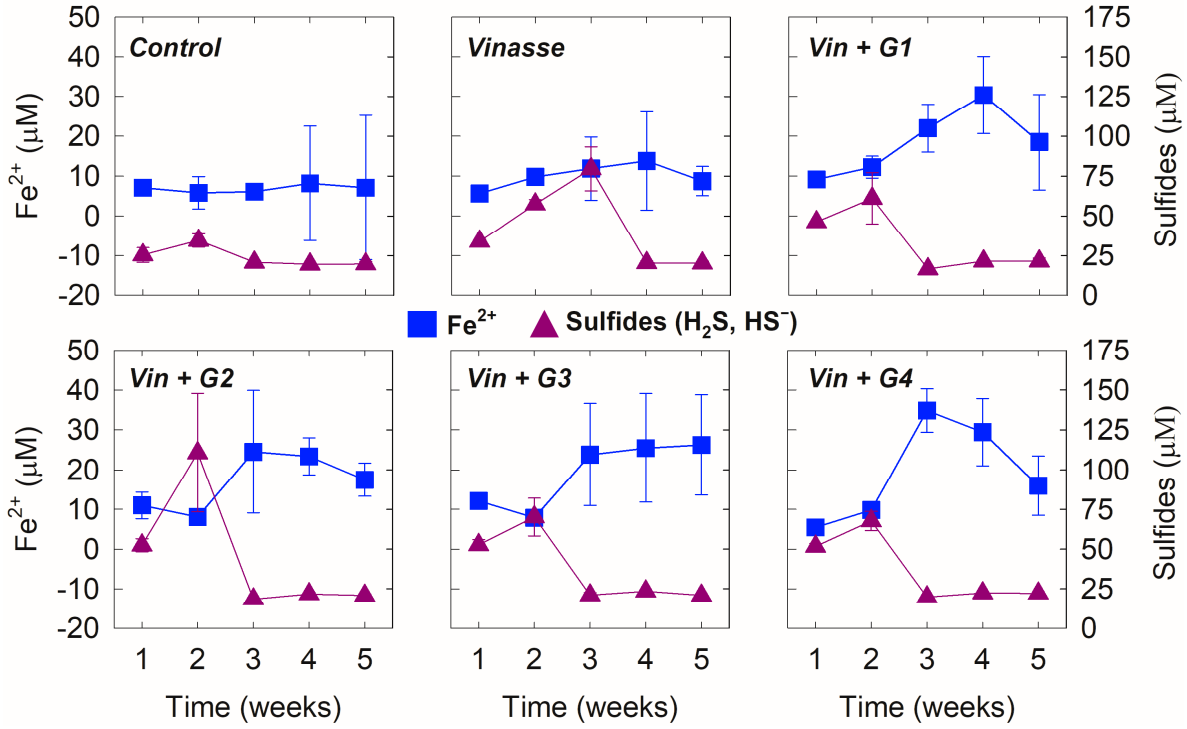

Figure 3. Fe^{2+} and sulfides (H_2S and HS^-) concentrations in the solution over time and depending on the addition of vinasse and gypsum doses. For interpretation of the references to color in this figure legend, the reader is referred to the web version of this article.

These behaviors of oxygen-sensitive chemical species (reduced iron, Fe^{2+}, and sulfide species, HS^- and H_2S) led to morphological changes over time (Figure 4) with an increase in gray and black spots in the mine tailings, especially in the treatments comprising gypsum and vinasse. Such changes are morphological evidence of sulfide formation [12]. In the vinasse only treatment the tailings were less red than those in the control treatment. In other words, there were more black spots in the treatments with vinasse and gypsum than in the treatments with vinasse only.

3.2. Variation of Solid-Phase Content over Time and as a Function of Amendment Dose

A larger decrease was observed in the pseudo-total Fe content when more sulfur was added (Figure 5), with Fe loss of −6.6% (Vin + G1), −13.6% (Vin + G2), −19.4% (Vin + G3), and −27.4% (Vin + G4). The decrease in pseudo-total Fe was associated with losses from oxide forms, mostly Fe-CR (on average −21%; Figure 6) which corroborates the Fe reduction process.

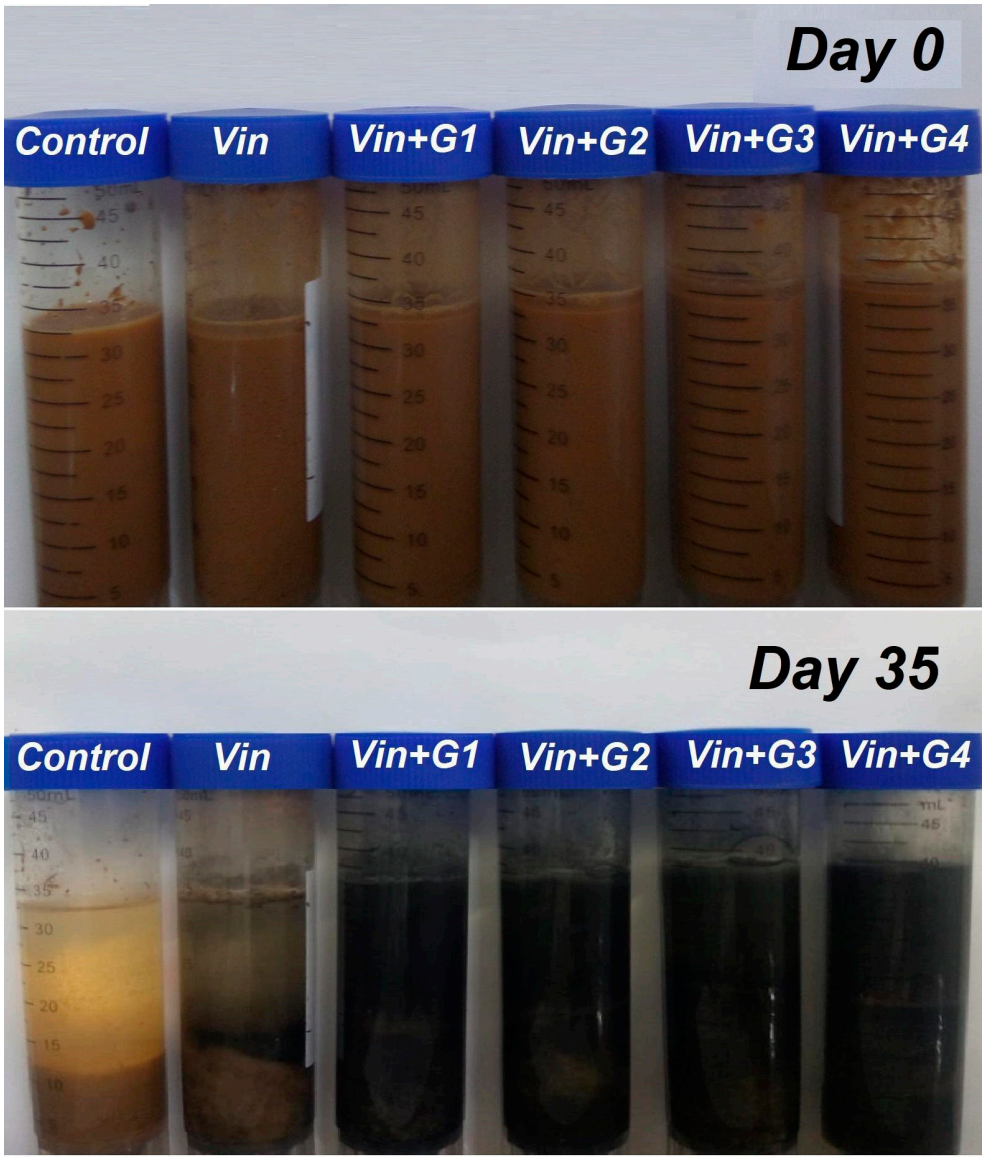

Figure 4. Experimental units at the start (day 0) and the end (day 35) of the trial. To analyze the colors of experimental units in this figure, the reader is referred to the web version of this article.

On the other hand, treatments with vinasse and gypsum enhanced the Fe content associated with carbonates (+784.1 $mg \cdot kg^{-1}$ or 50 times more Fe-CA than the control) and pyrite (+471.2 $mg \cdot kg^{-1}$ or 22 times more Fe-PY than the control). The Fe-CA increase was time-dependent: on average, there was 180 times more Fe-CA after 35 days of incubation than after 7 days of incubation. The increase in Fe-CA content in the mesocosm experiment may be a combination of CO_3^{2-} formation due to microbial respiration [45] and greater supply of Ca^{2+} from both gypsum and vinasse (Table 2). The CO_2 released from organic matter mineralization leads to the formation of CO_3^{2-} which in the presence of free Ca^{2+} precipitates as $CaCO_3$ [46,47]. The formation of carbonates (i.e., Fe-CA) may play a key role in metal immobilization since Fe-CA may be more stable mineral fraction than Fe oxyhydroxides in estuarine soil with limited pyritization processes [14,48].

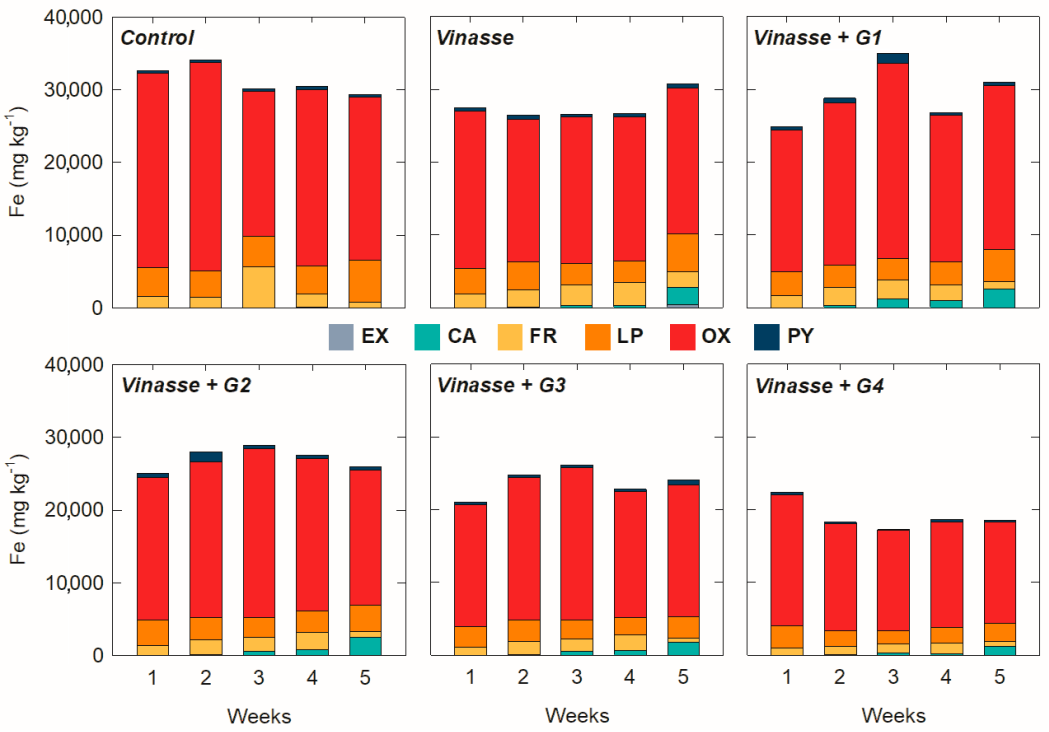

Figure 5. Fe solid-phase fractionation in mesocosm experiment over time. EX: Soluble and exchangeable Fe; CA: Fe associated with carbonates; FR: Fe associated with ferrihydrite; LP: Fe associated with lepidocrocite; CR: Fe associated with crystalline oxides; PY: Fe associated with pyrite. For interpretation of the references to color in this figure legend, the reader is referred to the web version of this article.

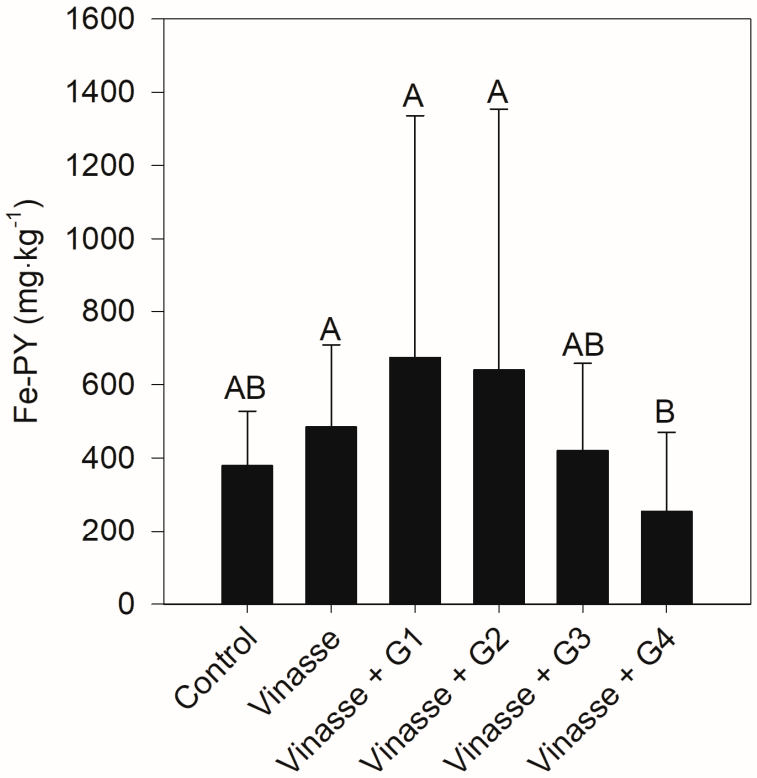

Figure 6. Fe content associated with pyrite (Fe-PY, mg kg^{-1}) in the function of the sulfur amendment. Means (n = 20) followed by the same letter did not differ significantly by the Kruskal–Wallis test ($p > 0.05$).

The increase in Fe associated with pyrite was dependent on the amount of S (Figure 6) and the highest amount of Fe-PY was obtained using 2 to 439 mg of S. These results indicate that even the sulfur content present in the vinasse (2 mg) may be sufficient to increase the pyritization in Fe-rich mining tailings deposited in the Doce River estuarine soil. In particular, in the present study on reactive Fe (i.e., a sum of Fe-EX to Fe-CR), the Fe/S ratio ranged from 3 to 919 (Table S2) revealing conditions favorable for pyritization [39,41], as several studies have reported that an Fe/S molar ratio above two favors the pyritization [40,41].

Fe oxides (Fe-FR, Fe-LP and Fe-OX) showed negative correlations with the amount of S added (Figure 7). On the other hand, high sulfur amendment contributes to a decrease in the concentration of Fe-oxides, resulting in a lower Fe pseudo-total content (Figure 5). The addition of sulfur leads to the formation of sulfides (Figure 4) and other sulfur species (for instance, sulfite ($S_2O_3^{2-}$) or elemental sulfur (S^0)) that are expected to reductively dissolve Fe(III) minerals, through the sulfidation process [11,40] according to the following reactions:

$$Fe^{3+} + S^{2-} \rightarrow Fe^{2+} + S^0 + e^- \quad (3)$$

$$S_2O_3^{2-} + 8Fe^{3+} + 5H_2O \rightarrow 2SO_4^{2-} + 8Fe^{2+} + 10H^+ \quad (4)$$

$$S^0 + 6Fe^{3+} + 4H_2O \rightarrow SO_4^{2-} + 6Fe^{2+} + 8H^+ \quad (5)$$

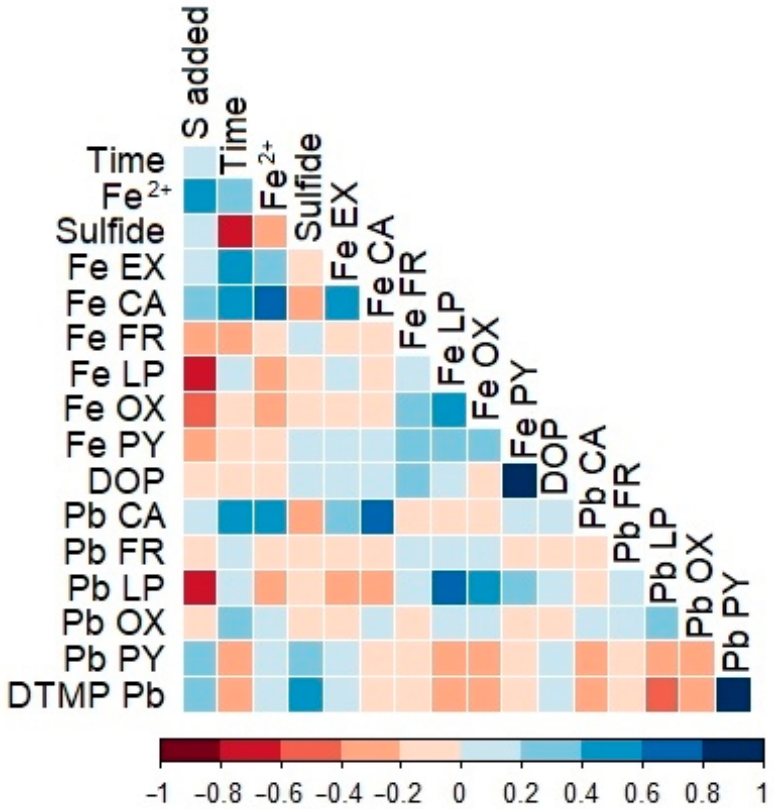

Figure 7. Spearman correlation color matrix between analyzed variables. Significances are shown in Table S3. S added: dose of sulfur added to the tubes (0, 2.4, 89.7, 439, 875 and 1748 mg); time: dates of evaluations (7, 14, 21, 28 and 35 days after treatments application); Fe^{2+}: concentration of Fe^{2+} in the solution, µM; sulfide: concentration of H_2S and HS^-, in the solution, µM; Fe and Pb-EX: exchangeable Fe and Pb, mg kg^{-1}; Fe and Pb-CA: Fe and Pb associated with carbonates, mg kg^{-1}; Fe and Pb-FR: Fe and Pb associated with ferrihydrite, mg kg^{-1}; Fe and Pb-LP: Fe and Pb associated with lepidocrocite, mg kg^{-1}; Fe and Pb-OX: Fe and Pb associated with hematite/goethite, mg kg^{-1}; Fe and Pb-PY: Fe and Pb associated with pyrite, mg kg^{-1}; DOP: degree of pyritization, % and DTMP-Pb: degree of trace metal pyritization of Pb, %. For interpretation of the references to color in this figure legend, the reader is referred to the web version of this article.

3.3. Pb Pyritization and Modeling

We evaluated Pb to assess the potential for other metals' pyritization. In the control treatment almost 45% of all Pb was already associated with pyrite, but the last 55% was mostly associated with iron oxides (Table S4), which can be reductively dissolved in estuarine conditions, mobilizing the trapped Pb.

Significantly higher Pb-DTMP was observed with the addition of gypsum (Figure 8), and there was a strong negative correlation (Figure 7) between Pb associated with lepidocrocite and the amount of S added to the mine tailings, indicating that the addition of gypsum affected the solid phase speciation of Pb, and Pb associated with lepidocrocite can be a source to Pb associated with pyrite. An addition of 439 mg of S was sufficient to raise the DTMP-Pb to 63%, lowering the labile or reactive Pb to less than TEL (35 mg·kg^{-1}). Similar results were obtained in a study using K_2SO_4 as a sulfate source to induce the formation of Pb sulfides in wetland tailings [11].

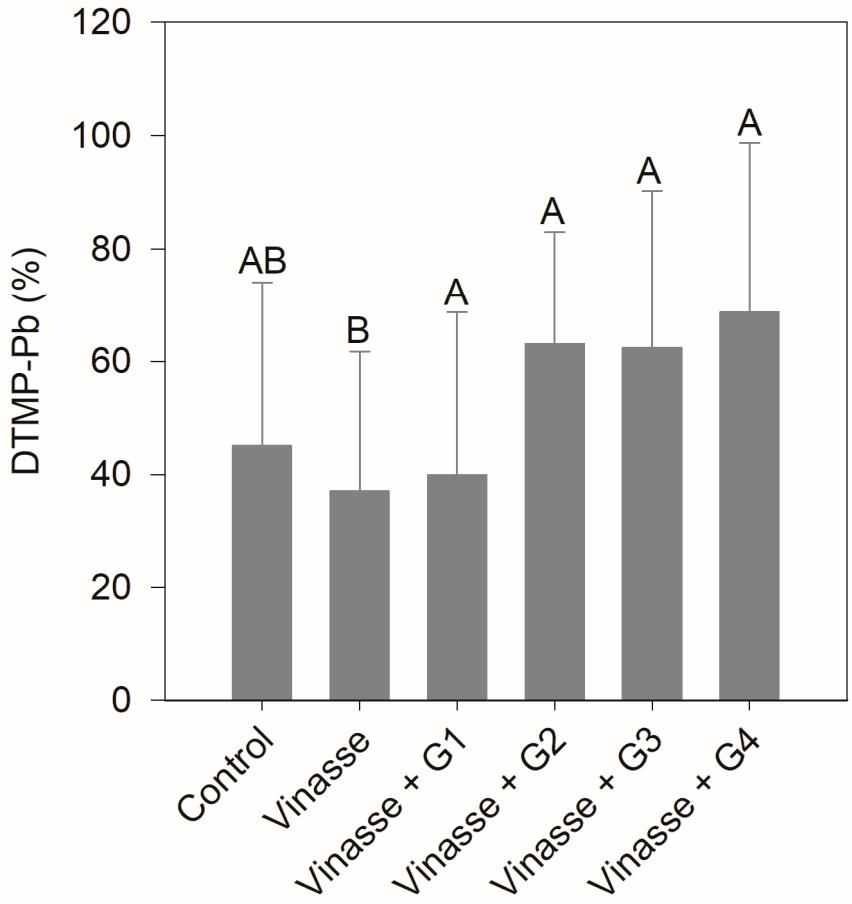

Figure 8. Degree of Pb pyritization (DTMP-Pb, %) as a function of sulfur amendment. Mean values (n = 20) followed by the same letter did not differ significantly by the Kruskal–Wallis test ($p > 0.05$).

Linear regression using the stepwise methodology resulted in two equations for modeling Pb pyritization, each one with DTMP-Pb and Pb-PY as dependent variables (Table 3). The selected equations had the highest conditional R^2 and highest Akaike's information criterion (AIC), minimizing data loss (Table 3). As expected, modeling showed that Pb pyritization is highly dependent on the sulfides content in the solution (Table 3) and this variable had the highest degree of fixed effects on Pb-PY and on the DTMP-Pb models. In addition, the degree of pyritization was highly relevant on Pb-pyritization. In other words, the precipitation of Pb with carbonates had negative effects on Pb pyritization, so in this batch experiment pyritization competed with the formation of carbonates (Table 3). This is corroborated by the high Fe-CA contents observed in the final weeks of experimenta-

tion with vinasse and gypsum addition (Figure 5) and the strong and positive correlation between Fe-CA and experiment time (Figure 7).

Table 3. Summary of the mixed-effect linear model for Pb pyritization obtained via stepwise backward elimination.

Variable	AIC *	R^2c **	Model (Significant Predictors in Bold, $p < 0.05$)
Pb-PY	341.04	0.73	Pb-PY= 49.32 × **Sulfides** + 13.32 × **DOP** + 0.0005 × **Fe-OX** − 2.29 × **Pb-CA** − 3.93
DTMP-Pb	467.55	0.53	DTMP-Pb= 248.48 × **Sulfides** +73.1 × **DOP** – 19 × **Pb-CA** + 9.87

* AIC: Akaike's information criterion; ** R^2c: conditional R squared; n = 90; units: Fe-OX, Pb-CA, and Pb-PY in mg·kg^{-1}, sulfides in µM; DOP and DTMP-Pb in %.

4. Conclusions

The results show that it is possible to increase the pyritization in Fe-rich mine tailings using sulfur amendments (e.g., gypsum and vinasse), since the concentration of Fe and Pb associated with pyrite increased in a short time (5 weeks) when compared with the control treatment. An optimum gypsum dose of 439 mg of S per 25 g of tailings was determined for increasing the pyritization of Fe and Pb. The results obtained in this study not only provide a base on which to design strategies for estuarine soil trace metal remediation and River Doce estuary reclamation, but also for other wet environments exposed to a huge amount of Fe. Future research should examine how to improve sulfate reduction (for instance, inoculation of the tailings with sulfate reducing bacteria) and consider the effects of real-world conditions (such as open atmosphere, tide effects, and long-term gypsum dissolution) to develop effective technologies and techniques.

Supplementary Materials: The following are available online at https://www.mdpi.com/2075-163X/11/2/201/s1, Figure S1: Bulk samples XRD patterns from recently mine tailing deposited at Doce river estuary, Table S1: Average, standard deviation and p-values from the Kruskal–Wallis test, Table S2: Reactive Fe (sum of Fe-EX to Fe-OX) and sulfide (H_2S and HS^-) molar ratio, Table S3: Correlation coefficients (in bold) and p-value of Spearman correlation analysis, Table S4: Pb solid-phase fractionation from the mesocosm experiment over time.

Author Contributions: Conceptualization, T.O.F. and A.D.F.; methodology, A.D.F. and M.P.K.; formal analysis, A.D.F. and H.M.Q.; writing—original draft preparation, A.D.F.; writing—review and editing, A.D.F., H.M.Q., G.N.N., X.L.O., Â.F.B., T.O.F.; project administration, Â.F.B. and T.O.F.; funding acquisition, Â.F.B. and T.O.F. All authors have read and agreed to the published version of the manuscript.

Funding: This work was funded by grants to AFB and TOF from Fundação de Amparo do Espirito Santo (FAPES/CNPq/CAPES Rio Doce 77683544/2017), Coordenação de Aperfeiçoamento de Pessoal de Nível Superior CAPES—Finance Code 001 and CNPq (grant numbers, AFB: 301161/2017-8, TOF: 305996/2018-5; GNN: 409593/2018-4). The authors are grateful for the financial support provided by São Paulo Research Foundation (FAPESP, ADF grant number 2019/14800-5, HMQ grant number 2018/04259-2; MPK grant number 2020/06224-1; TOF grant numbers 2019/19987-6 and 2018/08408-2). Xunta de Galicia-Consellería de Educación e Ordeanción Universitaria de Galicia (Consolidation of competitive groups of investigation; GRC GI 1574) and CRETUS strategic group (AGRUP2015/02). Fundação Carlos Chagas Filho de Amparo à Pesquisa do Estado do Rio de Janeiro (GNN, JCNE Grant E-26/202.757/2019).

Conflicts of Interest: The authors declare no conflict of interest. The funders had no role in the design of the study; in the collection, analyses, or interpretation of data; in the writing of the manuscript, or in the decision to publish the results.

References

1. Nóbrega, G.N.; Ferreira, T.O.; Neto, M.S.; Queiroz, H.M.; Artur, A.G.; Mendonça, E.D.S.; Silva, E.D.O.; Otero, X.L. Edaphic factors controlling summer (rainy season) greenhouse gas emissions (CO_2 and CH_4) from semiarid mangrove soils (NE-Brazil). *Sci. Total. Environ.* **2016**, *542*, 685–693. [CrossRef]
2. Machado, W.; Borrelli, N.; Ferreira, T.O.; Marques, A.; Osterrieth, M.; Guizan, C. Trace metal pyritization variability in response to mangrove soil aerobic and anaerobic oxidation processes. *Mar. Pollut. Bull.* **2014**, *79*, 365–370. [CrossRef]

3. Otero, X.L.; Ferreira, T.O.; Huerta-Diaz, M.A.; Partiti, C.S.D.M.; Souza, V.; Torrado, P.V.; Macías, F. Geochemistry of iron and manganese in soils and sediments of a mangrove system, Island of Pai Matos (Cananeia—SP, Brazil). *Geoderma* **2009**, *148*, 318–335. [CrossRef]
4. Andrade, R.A.; Sanders, C.J.; Boaventura, G.; Patchineelam, S.R. Pyritization of trace metals in mangrove sediments. *Environ. Earth Sci.* **2012**, *67*, 1757–1762. [CrossRef]
5. Berner, R.A. Sedimentary pyrite formation. *Am. J. Sci.* **1970**, *268*, 1–23. [CrossRef]
6. Huerta-Diaz, M.A.; Morse, J.W. Pyritization of trace metals in anoxic marine sediments. *Geochim. Cosmochim. Acta* **1992**, *56*, 2681–2702. [CrossRef]
7. Rickard, D.; Morse, J.W. Acid volatile sulfide (AVS). *Mar. Chem.* **2005**, *97*, 141–197. [CrossRef]
8. Ferreira, T.O.; Nóbrega, G.N.; Albuquerque, A.G.B.M.; Sartor, L.R.; Gomes, I.S.; Artur, A.G.; Otero, X. Pyrite as a proxy for the identification of former coastal lagoons in semiarid NE Brazil. *Geo-Mar. Lett.* **2015**, *35*, 355–366. [CrossRef]
9. Alongi, D.; Wattayakorn, G.; Boyle, S.; Tirendi, F.; Payn, C.; Dixon, P. Influence of roots and climate on mineral and trace element storage and flux in tropical mangrove soils. *Biogeochemistry* **2004**, *69*, 105–123. [CrossRef]
10. Hellige, K.; Pollok, K.; Larese-Casanova, P.; Behrends, T.; Peiffer, S. Pathways of ferrous iron mineral formation upon sulfidation of lepidocrocite surfaces. *Geochim. Cosmochim. Acta* **2012**, *81*, 69–81. [CrossRef]
11. Devolder, P.S.; Brown, S.L.; Hesterberg, D.; Pandya, K. Metal Bioavailability and Speciation in a Wetland Tailings Repository Amended with Biosolids Compost, Wood Ash, and Sulfate. *J. Environ. Qual.* **2003**, *32*, 851–864. [CrossRef] [PubMed]
12. Berkowitz, J.F.; Vanzomeren, C.M.; Fresard, N.D. Rapid formation of iron sulfides alters soil morphology and chemistry following simulated marsh restoration. *Geoderma* **2019**, *351*, 76–84. [CrossRef]
13. Carmo, F.F.D.; Kamino, L.H.Y.; Junior, R.T.; De Campos, I.C.; Carmo, F.F.D.; Silvino, G.; Castro, K.J.D.S.X.D.; Mauro, M.L.; Rodrigues, N.U.A.; Miranda, M.P.D.S.; et al. Fundão tailings dam failures: The environment tragedy of the largest technological disaster of Brazilian mining in global context. *Perspect. Ecol. Conserv.* **2017**, *15*, 145–151. [CrossRef]
14. Queiroz, H.M.; Nóbrega, G.N.; Ferreira, T.O.; Almeida, L.S.; Romero, T.B.; Santaella, S.T.; Bernardino, A.F.; Otero, X.L. The Samarco mine tailing disaster: A possible time-bomb for heavy metals contamination? *Sci. Total. Environ.* **2018**, 498–506. [CrossRef] [PubMed]
15. Gomes, L.E.D.O.; Correa, L.B.; Sá, F.; Neto, R.R.; Bernardino, A.F. The impacts of the Samarco mine tailing spill on the Rio Doce estuary, Eastern Brazil. *Mar. Pollut. Bull.* **2017**, *120*, 28–36. [CrossRef]
16. Gabriel, F.A.; Silva, A.G.; Queiroz, H.M.; Ferreira, T.O.; Hauser-Davis, R.A.; Bernardino, A.F. Ecological Risks of Metal and Metalloid Contamination in the Rio Doce Estuary. *Integr. Environ. Assess. Manag.* **2020**, *16*, 655–660. [CrossRef]
17. Bernardino, A.F.; Pais, F.S.; Oliveira, L.S.; Gabriel, F.A.; Ferreira, T.O.; Queiroz, H.M.; Mazzuco, A.C.A. Chronic trace metals effects of mine tailings on estuarine assemblages revealed by environmental DNA. *PeerJ* **2019**, *7*, e8042. [CrossRef]
18. Queiroz, H.M.; Ferreira, T.O.; Barcellos, D.; Nóbrega, G.N.; Antelo, J.; Otero, X.L.; Bernardino, A.F. From sinks to sources: The role of Fe oxyhydroxide transformations on phosphorus dynamics in estuarine soils. *J. Environ. Manag.* **2021**, *278*, 111575. [CrossRef]
19. Burton, J.G.A. Sediment quality criteria in use around the world. *Limnology* **2002**, *3*, 65–76. [CrossRef]
20. Lwin, C.S.; Seo, B.-H.; Kim, H.-U.; Owens, G.; Kim, K.-R. Application of soil amendments to contaminated soils for heavy metal immobilization and improved soil quality—A critical review. *Soil Sci. Plant Nutr.* **2018**, *64*, 156–167. [CrossRef]
21. Andrunik, M.; Wołowiec, M.; Wojnarski, D.; Zelek-Pogudz, S.; Bajda, T. Transformation of Pb, Cd, and Zn Minerals Using Phosphates. *Minerals* **2020**, *10*, 342. [CrossRef]
22. Guo, G.; Zhou, Q.; Ma, L.Q. Availability and Assessment of Fixing Additives for The in Situ Remediation of Heavy Metal Contaminated Soils: A Review. *Environ. Monit. Assess.* **2006**, *116*, 513–528. [CrossRef] [PubMed]
23. Evans, K. The History, Challenges, and New Developments in the Management and Use of Bauxite Residue. *J. Sustain. Met.* **2016**, *2*, 316–331. [CrossRef]
24. Mahmoodabadi, M.; Yazdanpanah, N.; Sinobas, L.R.; Pazira, E.; Neshat, A. Reclamation of calcareous saline sodic soil with different amendments (I): Redistribution of soluble cations within the soil profile. *Agric. Water Manag.* **2013**, *120*, 30–38. [CrossRef]
25. Seixas, F.L.; Gimenes, M.L.; Fernandes, N.R. Treatment of vinasse by adsorption on carbon from sugar cane bagasse. *Química Nova* **2016**, *39*, 172–179. [CrossRef]
26. Gee, G.W.; Bauder, J.W. Particle-Size Analysis. In *Methods of Soil Analysis: Part 1—Physical and Mineralogical Methods*; Soil Science Society of America, American Society of Agronomy: Madison, WI, USA, 1986; pp. 383–411.
27. Howard, J.; Hoyt, S.; Isensee, K.; Pidgeon, E. *Maciej Telszewski Coastal Blue Carbon: Methods for Assessing Carbon Stocks and Emissions Factors in Mangroves, Tidal Salt Marshes, and Seagrass Meadows*, 1st ed.; International Union for Conservation of Nature (IUCN): Arlington, VA, USA, 2014.
28. USEPA. *Method 3052: Microwave Assisted Acid Digestion of Siliceous and Organically Based Matrices*; United States Environmental Protection Agency: Washington, DC, USA, 1996.
29. USEPA. *Method 6010C Inductively Coupled Plasma-Atomic Emission Spectometry*; United States Environmental Protection Agency: Washington, DC, USA, 1997; Volume 2, pp. 1–19.
30. MAPA, *Instrução Normativa n. 027 de 05 de Junho de 2006. Dispõe Sobre Fertilizantes, Corretivos, Inoculantes e Biofertilizantes, Para Serem Produzidos, Importados Ou Comercializados, Deverão Atender Aos Limites Estabelecidos Nesta Instrução*; Esplanada dos Ministérios Bloco D-Brasília: Brasília Brazil, 2006.

31. Viollier, E.; Inglett, P.; Hunter, K.; Roychoudhury, A.; Van Cappellen, P. The ferrozine method revisited: Fe(II)/Fe(III) determination in natural waters. *Appl. Geochem.* **2000**, *15*, 785–790. [CrossRef]
32. Cline, J.D. Spectrophotometric determination of hydrogen sulfide in natural waters. *Limnol. Oceanogr.* **1969**, *14*, 454–458. [CrossRef]
33. Huerta-Diaz, M.A.; Morse, J.W. A quantitative method for determination of trace metal concentrations in sedimentary pyrite. *Mar. Chem.* **1990**, *29*, 119–144. [CrossRef]
34. Fortin, D.; Leppard, G.G.; Tessier, A. Characteristics of lacustrine diagenetic iron oxyhydroxides. *Geochim. Cosmochim. Acta* **1993**, *57*, 4391–4404. [CrossRef]
35. Tessier, A.; Campbell, P.G.C.; Bisson, M. Sequential extraction procedure for the speciation of particulate trace metals. *Anal. Chem.* **1979**, *51*, 844–851. [CrossRef]
36. Ferreira, T.O.; Otero, X.L.; Vidal-Torrado, P.; Macías, F. Redox Processes in Mangrove Soils under Rhizophora mangle in Relation to Different Environmental Conditions. *Soil Sci. Soc. Am. J.* **2007**, *71*, 484–491. [CrossRef]
37. Reimann, C.; Filzmoser, P.; Garrett, R.G.; Dutter, R. *Statistical Data Analysis Explained*; John Wiley & Sons, Ltd.: Chichester, UK, 2008; ISBN 9780470987605.
38. *RStudio Team*; RStudio: Boston, MA, USA, 2020.
39. Peiffer, S.; Behrends, T.; Hellige, K.; Larese-Casanova, P.; Wan, M.; Pollok, K. Pyrite formation and mineral transformation pathways upon sulfidation of ferric hydroxides depend on mineral type and sulfide concentration. *Chem. Geol.* **2015**, *400*, 44–55. [CrossRef]
40. Wan, M.; Schröder, C.; Peiffer, S. Fe(III):S(-II) concentration ratio controls the pathway and the kinetics of pyrite formation during sulfidation of ferric hydroxides. *Geochim. Cosmochim. Acta* **2017**, *217*, 334–348. [CrossRef]
41. Kumar, N.; Lezama-Pacheco, J.; Noël, V.; Dublet, G.; Brown, G.E. Sulfidation mechanisms of Fe(iii)-(oxyhydr)oxide nanoparticles: A spectroscopic study. *Environ. Sci. Nano* **2018**, *5*, 1012–1026. [CrossRef]
42. Burton, E.D.; Bush, R.T.; Sullivan, L.A. Fractionation and extractability of sulfur, iron and trace elements in sulfidic sediments. *Chemosphere* **2006**, *64*, 1421–1428. [CrossRef] [PubMed]
43. Nóbrega, G.N.; Ferreira, T.O.; Romero, R.E.; Marques, A.G.B.; Otero, X. Iron and sulfur geochemistry in semi-arid mangrove soils (Ceará, Brazil) in relation to seasonal changes and shrimp farming effluents. *Environ. Monit. Assess.* **2013**, *185*, 7393–7407. [CrossRef] [PubMed]
44. Noël, V.; Marchand, C.; Juillot, F.; Ona-Nguema, G.; Viollier, E.; Marakovic, G.; Olivi, L.; Delbes, L.; Gelebart, F.; Morin, G. EXAFS analysis of iron cycling in mangrove sediments downstream a lateritized ultramafic watershed (Vavouto Bay, New Caledonia). *Geochim. Cosmochim. Acta* **2014**, *136*, 211–228. [CrossRef]
45. Lian, B.; Hu, Q.; Chen, J.; Ji, J.; Teng, H.H. Carbonate biomineralization induced by soil bacterium Bacillus megaterium. *Geochim. Cosmochim. Acta* **2006**, *70*, 5522–5535. [CrossRef]
46. Dhami, N.K. Biomineralization of Calcium Carbonate Polymorphs by the Bacterial Strains Isolated from Calcareous Sites. *J. Microbiol. Biotechnol.* **2013**, *23*, 707–714. [CrossRef]
47. Castanier, S.; Le Métayer-Levrel, G.; Perthuisot, J.-P. Bacterial Roles in the Precipitation of Carbonate Minerals. In *Microbial Sediments*; Springer: Berlin/Heidelberg, Germany, 2000; pp. 32–39.
48. Sundaray, S.K.; Nayak, B.B.; Lin, S.; Bhatta, D. Geochemical speciation and risk assessment of heavy metals in the river estuarine sediments—A case study: Mahanadi basin, India. *J. Hazard. Mater.* **2011**, *186*, 1837–1846. [CrossRef]